Probe spacing optimization to reduce the F3S straightness measurement uncertainty based on spacing uncertainty propagation law

Pu Huang[1], Jin Xie[1], Zhiguang Liu[1], Zhilin He[1], Xuancheng Huang[1], Shengyu Shi[*,1]

1. School of Mechanical and Automobile Engineering, South China University of Technology, Guangzhou, 510640, P.R. China
Email addresses: shisy@scut.edu.cn (S. Shi)

KEYWORDS: F3S straightness measurement; Spacing uncertainty propagation; Monte Carlo method; Spacing optimization

The Fourier three-sensor (F3S) straightness measurement is a promising on-machine measurement of the slide error motion by eliminating the influence of the workpiece profile. However, in the F3S measurement, the probe spacing deviation deteriorates the measurement accuracy significantly. Up to now, it still lacks an effective method to reduce the influence of spacing uncertainty in the F3S measurement. Thus, a novel method will be proposed to improve measurement accuracy in this paper. To get this target, first, the algorithm of the F3S method based on the Laplace transform was reviewed. Then, we theoretically analyzed the adverse impact of the probe spacing deviation. Next, to quantify the influence of the spacing uncertainty, we algebraically derived the spacing uncertainty propagation law based on the partial differential in the S domain. Subsequently, to reduce the measurement uncertainty, a solution of spacing optimization is presented based on the uncertainty propagation law. Finally, to validate the effect of the spacing optimization, Monte Carlo simulations were performed. The results show that the derived uncertainty agrees well with the statistical uncertainty with an error of 0.6 μm (6%). Moreover, the F3S measurement can achieve the smallest uncertainty by the spacing optimization based on the derived uncertainty.

NOMENCLATURE

m_1, m_2, m_3 = signal of the probes P_1, P_2, and P_3.
d = the spacing between P_1 and P_2
L = the length of measurement section
$f(\theta)$ = the workpiece profile
$g(\theta)$ = the slide error motion
θ = the equivalent angular position of the probe P_1
$m(\theta)$ = the weighted function
$F(s)$, $G(s)$, and $M(s)$ = the Laplace transform of $f(\theta)$, $g(\theta)$, and $m(\theta)$
k = the number of order
$F(jk)$, $G(jk)$, and $M(jk)$ = Fourier transform of $f(\theta)$, $g(\theta)$, and $m(\theta)$
$T(jk)$ = the transfer function from $M(jk)$ to $F(jk)$.
$U_h(k)$ = the harmonic uncertainty
$U_H(k)$ = the overall harmonic uncertainty
U = the spatial measurement uncertainty

1. Introduction

There is an increasing need for optical lenses with high imaging performance and long lifespans [1,2]. However, when machining optical lenses on brittle materials, unstable cutting depths may produce brittle fractures, thus, generating a thick subsurface damage layer, and deteriorating the service life and focusing capability [3-5].

In general, unstable cutting depths may arise from the error motion of the linear slide and the rotary spindle of the grinding machine used [6, 7]. Hence it can be expected that compensating for the slide error motion can reduce the profile error and subsurface damage layer to a certain extent [8]. To achieve this aim, the first step is to precisely evaluate the slide error motion.

For efficiency issues, on-machine measurement has become one of

* Corresponding author. Tel.: 0086 (020) 87114578; Fax: 0086 (020) 87112503

the most popular methods to assess slide error motion. Commonly, in the on-machine measurement of slide error motion, a probe is mounted on the slide, then reads runout signals of a reference workpiece. The runout signals are always regarded as the slide error motion by neglecting the workpiece profile error. However, the workpiece profile error can be superposed into the probe signal when the workpiece profile is at the same level as the slide error motion, which is the main source of the measurement error.

To tackle this issue, straightness error separation techniques, which can simultaneously assess the two quantities, have been investigated since the 1970s [10, 11]. In the 1980s, Tanaka [12] developed the sequential two-point (S-2P) method, which utilized two sensors/probes mounted in a row that moved together to measure at two positions with an interval of spacing between the two probes. The slide error motion and workpiece straightness were then computed by an iterative accumulation of the differential output. Then, Tanaka [13] also pointed out that the yaw angle of the slide was involved in the probe signal, and to simultaneously compute the three quantities, he employed a third probe to the S-2P method, which was called the sequential three-point (S-3P) method. However, the probe spacing cannot be smaller than their sizes as they interfere, the lateral resolution of the measurement is limited in these two methods. Thus, the high-frequency components of the profile cannot be evaluated.

To enhance the lateral resolution, Li [14] applied two capacitive displacement probes to dynamically collect the runout signal and separate the workpiece profile and slide error motion using the Discrete Fourier transform (DFT), which was the Fourier two-sensor (F2S) method. However, he also stated that an unexpected deviation can occur in the estimation if the workpiece profile periodically occurs with a period of the distance between the two probes.

To overcome the non-periodic issue, Fung [15] applied a third probe to the F2S method to rectify the probe signal. This method is called the Fourier 3-sensor (F3S) method and was later verified as applicable [16].

However, the F3S measurement faces three main challenges: the height difference between the second and third probes, the probe stochastic noise (probe uncertainty) [16], and the probe spacing uncertainty, each of which can significantly affect the measurement precision. In our previous paper [16], we proposed a solution to estimate and compensate for the height difference and used the criteria of the determinant of transfer matrix $|W(k)|$ to measure the harmonic uncertainty caused by probe noise. Based on this, a hybrid F3S method was developed to alleviate the stochastic uncertainty by performing several F3S measurements under different probe spacings and selecting the optimal Fourier coefficients of the straightness profile individually from the several candidate F3S measurements in accordance with the maximal $|W(k)|$.

However, few studies have investigated the influence of the probe spacing uncertainty on the F3S measurement, especially the spacing error propagation law. And there still lacks methods to reduce the adverse impact of the probe spacing uncertainty. Therefore, this paper aims to develop an effective method to quantitatively estimate the measurement uncertainty, which is introduced by the spacing uncertainty; then, develop a solution to cancel the measurement uncertainty.

The rest of this paper is organized as follows. In Section 2, an algorithm of the F3S method based on the Laplace transform will be described. In Section 3, the adverse effect of the spacing deviation between the first and the second probes will be analyzed; and then, the spacing uncertainty propagation law will be algebraically derived by partial differential in the S domain; finally, to reduce the measurement uncertainty, a solution of spacing optimization will be developed based the uncertainty propagation law. In Section 4, to verify the effect of the spacing optimization, the Monte Carlo simulations will be conducted. The conclusions are drawn in Section 5.

2. Principle of the F3S straightness measurement

2.1 Laplace-transform-based algorithm of the F3S method

Fig. 1 shows the schematic diagram of the F3S straightness measurement. To measure the slide error motion of the measurement section between M_1 and M_2, three displacement probes P_1, P_2 and P_3 are applied and mounted on a linear moving slide of the X-axis of a machine by a fixture. It should be noted that: the separating spacing between P_2 and P_3 constantly equals the length of measurement section L; P_1 is installed between P_2 and P_3 with a spacing of d to P_2.

When the measurement starts, P_1 moves from M_1 to M_2, together with the other two probes, and three readings are taken. The readings of P_1, P_2 and P_3 are defined as $m_1(\theta)$, $m_2(\theta)$ and $m_3(\theta)$.

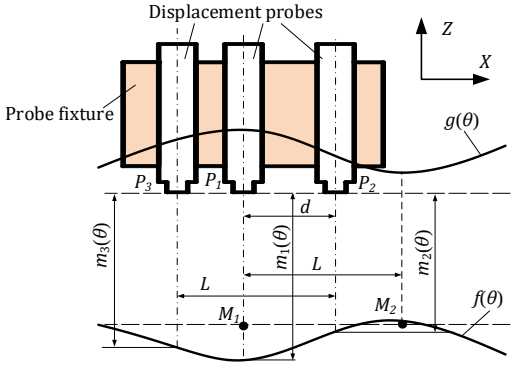

Fig. 1. Schematic diagram of F3S straightness measurement.

To solve the nonlinear issue of the straightness measurement by the F2S method, the part of $m_2(\theta)$ from the beginning of sampling to the time P_2 arriving at M_2 is cut off as $m_2'(\theta)$; the part of $m_3(\theta)$ from the time P_2 arriving at M_2 to the end of sampling is cut off as $m_3'(\theta)$; then, $m_3'(\theta)$ is emerged to $m_2'(\theta)$ as the rectified signal $m_{r2}(\theta)$. Thus, the probe readings can be written mathematically as follows:

$$m_1(\theta) = f(\theta) + g(\theta),\ (0 \le \theta < 2\pi) \tag{1}$$

$$m_{r2}(\theta) = \begin{cases} m_2'(\theta) = f\left(\theta + \frac{2\pi d}{L}\right) + g(\theta), \\ \left(0 \le \theta < \frac{2\pi d}{L} - 2\pi\right) \\ m_3'(\theta) = f\left(\theta + \frac{2\pi d}{L} - 2\pi\right) + g(\theta), \\ \left(\frac{2\pi d}{L} - 2\pi \le \theta < 2\pi\right) \end{cases} \tag{2}$$

respectively. Here, $g(\theta)$ and $f(\theta)$ represent the slide error motion

and the workpiece profile, respectively; θ is the equivalent angular position of the probe P_1, which is expressed as $\theta = \frac{2\pi x}{L}$; x is the actual position of P_1 along the X-axis.

Clearly, from Eq. (1) and (2), the probe readings m_1 and m_{r2} are both superposed of the slide error motion $g(\theta)$ and the workpiece profile $f(\theta)$. Moreover, m_2 contains a phase shift $\frac{2\pi d}{L}$ caused by the Probe P_2 position. Then, to calculate $g(\theta)$, several steps are required, as follows.

Step 1. Eliminate the influence of slide error motion $g(\theta)$ by subtract $m_{r2}(\theta)$ from $m_1(\theta)$:

$$m(\theta) = m_1(\theta) - m_{r2}(\theta) = f(\theta) - f(\theta + \frac{2\pi d}{L}) \quad (3)$$

Here, $m(\theta)$ is usually called the weighted function. However, the phase shift $\frac{2\pi d}{L}$ still damage the result.

Step 2. Remove the impact of the phase shift $\frac{2\pi d}{L}$ by employing the Laplace transform to Eq. (3):

$$F(s) = \frac{1}{1-e^{-\frac{2\pi d}{L}s}} M(s) \quad (4)$$

Here, $F(s)$ and $M(s)$ are the Laplace transform of $f(\theta)$ and $m(\theta)$, respectively.

Step 3. Transform the Laplace transform into Fourier transform by substituting $s = jk$ into Eq. (4):

$$F(jk) = \frac{1}{1-e^{j\frac{2\pi d}{L}k}} M(jk) \quad (5)$$

Here, $F(jk)$ and $M(jk)$ are Fourier transform of $f(\theta)$ and $m(\theta)$, respectively. k is the harmonic order, which equals ⋯, -2, -1, 0, 1, 2, ⋯. Thus, $f(\theta)$ is easily assessed by applying inverse discrete Fourier transform to Eq. (5).

The transfer function from $M(jk)$ to $F(jk)$ can be described as:

$$T(jk) = \frac{1}{1-e^{j\frac{2\pi d}{L}k}} \quad (6)$$

Step 4. Apply the inverse discrete Fourier transform to $F(jk)$:

$$f(\theta) = F^{-1}[F(jk)] \quad (7)$$

In this way, the workpiece profile $f(\theta)$ is finally estimated.

Step 5. Calculate the slide error motion by subtracting $f(\theta)$ from $m_1(\theta)$ as follows:

$$g(\theta) = m_1(\theta) - f(\theta) \quad (8)$$

Thus, the slide error motion can be exactly assessed.

3. Reduction of the F3S measurement uncertainty introduced by deviation of the probe spacing

3.1 The influence of probe spacing deviation on measurement accuracy

To measure the target section of the slide error motion $g(\theta)$, the positions of P_2 and P_3 keep constant on the fixture in the F3S measurement. And the spacing always equals the length of the measurement section L. Thus, in this paper, we assume that the spacing between the P_2 and P_3 is ideal, and only the adverse influence of the deviation of the spacing between P_1 and P_2 is estimated.

Fig. 2 shows the effect of the spacing deviation between P_1 and P_2. The nominal dimension of the spacing between P_1 and P_2 is designed as d. But to facilitate ease of transport, the probes are frequently mounted and unmounted. Due to the machining error of the probe mounting hole on the fixture, there is a spacing deviation Δd between P_1 and P_2, which is randomly changed with each probe mounting operation, as shown in Fig. 2(a).

As Eq. (6) describes, under ideal conditions without spacing deviation, the transfer function $T(jk) = \frac{1}{1-e^{j\frac{2\pi d}{L}k}}$ is applied when calculating the slide error motion $g(\theta)$, as the black route in Fig. 2(b). However, the probe spacing deviation Δd introduces a phase error $\frac{2\pi \Delta d}{L}$ of the transfer function. The actual transfer function is $T(jk) = \frac{1}{1-e^{j\frac{2\pi(d+\Delta d)}{L}k}}$, which should be employed in computing the slide error motion $g(\theta)$, which is shown by the red route in Fig. 2(b). Due to the spacing deviation Δd is random and hard to evaluate, it is commonly neglected in actual measurement. Thus, the ideal condition is assumed, and wrongly apply the black calculating route in Fig. 2(b). As a result, a measurement error occurs.

3.2 Reduction of the influence of the probe spacing deviation on the F3S measurement

To enhance the accuracy of F3S measurement by mitigating the impact of spacing deviation, a critical step is to evaluate the quantitative effect of probe spacing deviation and uncertainty propagation law. Hence, in this subsection, based on the systematic theory, the uncertainty propagation law will be derived.

Step 1, calculate the change rate of the estimated error of the slide error motion $g(\theta)$.

The estimated error of the slide error motion $g(\theta)$ in the S domain is assumed to be $\Delta G(s)$, which is introduced by the spacing deviation Δd. The change rate of the estimated error of the slide error motion $G(s)$ in the S domain:

$$E_{rate} = \frac{\Delta G(s)}{\Delta d} \quad (9)$$

Step 2, the partial derivation of $G(s)$ is introduced.

For the continuous variation of the $\Delta G(s)$ with the spacing deviation Δd, there is the algebraic limit of E_{rate} when Δd close to zero. Then, the error change rate E_{rate} can be written as:

$$\lim_{\Delta d \to 0} E_{rate} = \lim_{\Delta d \to 0} \frac{\Delta G(s)}{\Delta d} = \frac{d}{\partial d} G(s) \quad (10)$$

Thus, the partial differential of the slide error motion with respect to the probe spacing d in the S domain is introduced.

Step 3, the partial differential of the slide error motion is calculated.

From Eq. (8), the partial differential of the slide error motion in S domain can be derived as:

$$\frac{d}{\partial d} G(s) = \frac{d}{\partial d} M_1(s) - \frac{d}{\partial d} F(s) \quad (11)$$

Here, $M_1(s)$ and $F(s)$ is the Laplace transform of $m_1(\theta)$ and $f(\theta)$, respectively.

From Eqs. (4) and (11), the partial differential of the slide error motion is deduced as:

$$\frac{d}{\partial d} G(s) = \frac{d}{\partial d} M_1(s) + \frac{2\pi s}{L} e^{-\frac{2\pi d s}{L}} \frac{1}{\left(1-e^{-\frac{2\pi d s}{L}}\right)^2} M(s) = \frac{d}{\partial d} M_1(s) + \frac{2\pi d s}{L} e^{-\frac{2\pi d s}{L}} \frac{1}{1-e^{-\frac{2\pi d s}{L}}} F(s) \quad (12)$$

Due to Probe P_1 constantly moves from M_1 to M_2, $m_1(\theta)$ doesn't vary with Δd. Thus, $\frac{d}{\partial d} M_1(s)$ equals 0. Thus, Eq. (12) can be improved as:

$$\frac{d}{\partial d} G(s) = \frac{2\pi d s}{L} e^{-\frac{2\pi d s}{L}} \frac{1}{1-e^{-\frac{2\pi d s}{L}}} F(s) \quad (13)$$

In order to investigate the estimated error in the harmonic domain,

we take $s = jk$, so the Laplace transform is transferred to the Fourier transform as:

$$\frac{\partial}{\partial d}G(jk) = -\frac{j2\pi dk}{L}e^{-\frac{j2\pi dk}{L}}\frac{1}{1-e^{-j\frac{2\pi dk}{L}}}F(jk) \quad (14)$$

To make it easier to study the relationship between the estimated error and the probe spacing deviation, Eq. (14) can be written as:

$$\partial G(jk) = F(jk)\frac{j2\pi dk}{L}\frac{1}{1-e^{-j\frac{2\pi dk}{L}}}\partial d \quad (15)$$

Thus, the partial differential of the slide error motion $G(jk)$ with respect to the probe spacing d can be evaluated.

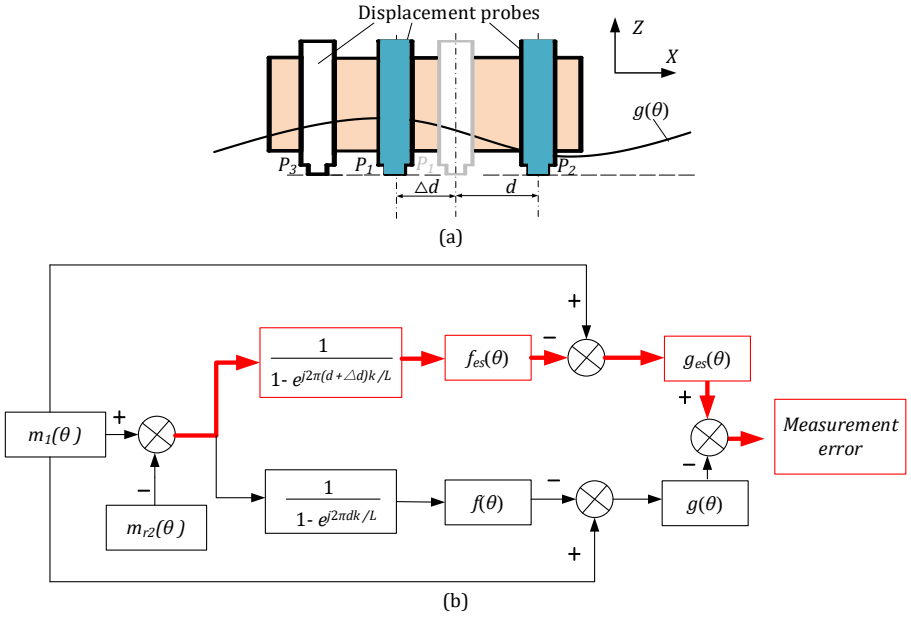

Fig. 2. The adverse effect of the spacing deviation between P_1 and P_2 in the F3S measurement: (a) the probe spacing deviation, and (b) the resulting error.

Step 4, the harmonic uncertainty of slide error motion is derived.

According to the ISO standard Supplement to GUM [17], the harmonic uncertainty can be defined as the standard deviation of the harmonic amplitude. Thus, from Eq. (15), the harmonic uncertainty $U_h(k)$ can be derived as:

$$U_h(k) = E\{|\partial G(jk)|\} = |F(jk)|\frac{2\pi dk}{L}\left|\frac{e^{-\frac{j2\pi dk}{L}}}{1-e^{-j\frac{2\pi dk}{L}}}\right|\sigma_d \quad (16)$$

Here, σ_d is the standard deviation of the probe spacing.

Thus, the overall harmonic uncertainty can be calculated as:

$$U_H(k) = \sqrt{\sum_{k=1}^{N_{cut-off}}[U_h(k)]^2} = \sqrt{\sum_{k=1}^{N_{cut-off}}\left[|F(jk)|\frac{2\pi dk}{L}\left|\frac{e^{-\frac{j2\pi dk}{L}}}{1-e^{-j\frac{2\pi dk}{L}}}\right|\sigma_d\right]^2} \quad (17)$$

Here, $N_{cut-off}$ is the cut-off harmonic.

Due to unvaried measurement section and machining errors of the fixture, $|F(jk)|$ and σ_d keep constant, respectively. Therefore, the overall harmonic uncertainty can be simplified as:

$$U_H(k) = \sqrt{\sum_{k=1}^{N_{cut-off}}\left[\frac{2\pi dk}{L}\left|\frac{1}{1-e^{-j\frac{2\pi dk}{L}}}\right|\right]^2} \quad (18)$$

Step 5, reduce measurement uncertainty by optimizing the probe spacing.

From Eq. (18), it is easy to know that the overall harmonic uncertainty related to the probe spacing d. Thus, an optimized probe spacing d_{op} can be achieved when overall harmonic uncertainty is the lowest, which can be described as:

$$d_{op} = argmin\{U_H(k)\} = argmin\left\{\sqrt{\sum_{k=1}^{N_{cut-off}}\left[\frac{2\pi dk}{L}\left|\frac{1}{1-e^{-j\frac{2\pi dk}{L}}}\right|\right]^2}\right\} \quad (19)$$

In this way, we can acquire the highest measurement accuracy by applying the optimized spacing d_{op} in F3S measurements.

4. Simulation verification

4.1 Simulation conditions

For verification of the method to reduce the measurement uncertainty, which is introduced by the spacing uncertainty, numerical simulations are carried out. In the simulations, the workpiece profile and the slide error motion are given as follows:

$$\overline{f(\theta)} = \sum_{k=1}^{N} 6e^{-0.08k}\cos(k\theta + \varphi_{kf}), (0 \le \theta < 2\pi) \quad (20)$$

$$\overline{g(\theta)} = \sum_{k=1}^{N} 4e^{-0.12k}\cos(k\theta + \varphi_{kg}), (0 \le \theta < 2\pi) \quad (21)$$

Here, $\overline{f(\theta)}$ and $\overline{g(\theta)}$ are the given actual workpiece profile and the actual slide error motion, respectively; φ_{kf} and φ_{kg} are harmonic phases of the k^{th} harmonic, which are taken randomly; and N is the cut-off harmonic, in this paper N=30.

Fig. 3 demonstrates the actual workpiece profile and the actual slide error motion. The measurement section was from 0 to 100 mm, namely, L = 100 mm. And d = 21.4 mm. To ensure the reliability, the simulations were performed 1000 times. To simulate the actual condition, the probe spacing deviation Δd was given randomly in each measurement, and Δd obeyed the normal distribution. In each time of the simulation, we also calibrated the probe spacing, and we counted the frequency of Δd, wherein $\Delta d \sim N(0, 0.39\ \mu m^2)$.

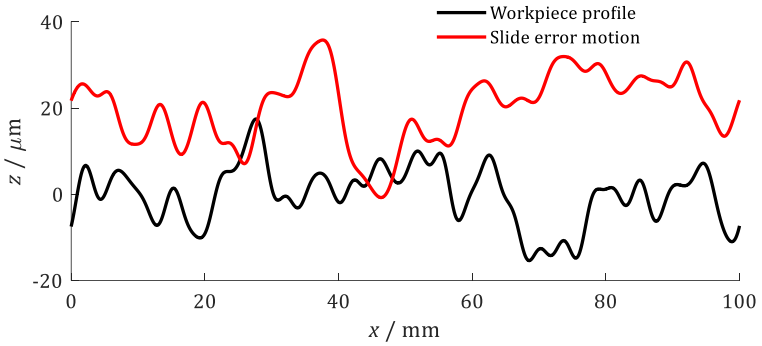

Fig. 3. The actual workpiece profile and the slide error motion.

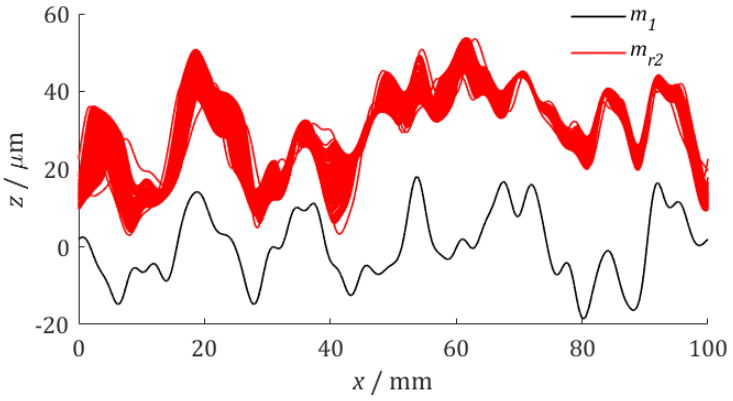

Fig. 4. The probe signals.

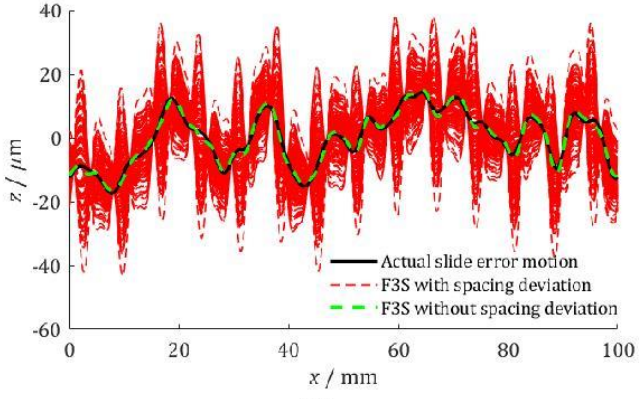

(a)

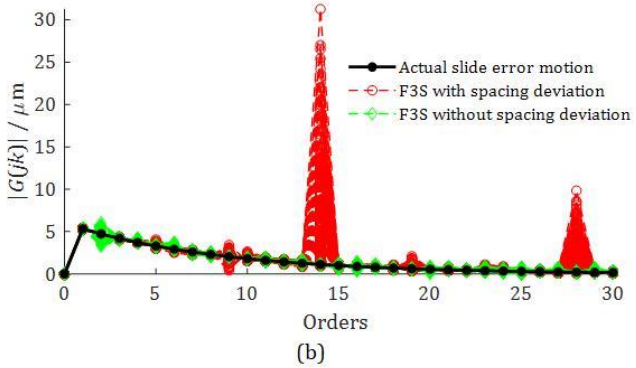

(b)

Fig. 5. The adverse impact of the spacing uncertainty on the F3S measurement.

4.2 Demonstration of the adverse influence of the spacing deviation on measurement accuracy

The probe signals are shown in Fig. 4. Due to the spacing deviation, the rectified signals m_{r2}, which is composed of second and third probe signals, are dispersive.

Fig.5 shows the results of the F3S measurement when d equals 21.4 mm. The slide error motion, which is estimated by the F3S measurement without spacing uncertainty, greatly agrees with the actual one both in spatial (see Fig. 5 (a)) and harmonic domain (see Fig. 5 (b)). Thus, the F3S method can precisely assess the slide error motion by canceling the influence of the workpiece profile. However, when there is spacing uncertainty, the estimated slide error motion curves disperse randomly with a fluctuating error of 25 μm in the spatial domain, as shown in Fig. 5(a); in the harmonic domain, large deviations at some harmonics: 14th and 28th harmonics. This suggests that the spacing uncertainty leads to the large estimated harmonics error and the spatial fluctuating errors.

4.3 Numerical verification of the probe spacing uncertainty propagation law

In the ISO standard Supplement to GUM [17], the Monte Carlo method, which has been considered one of the most powerful tools to assess the impact of multiple factors, is applied to count the measurement uncertainty. Hence, to validate the spacing uncertainty propagation law, Monte Carlo simulation is performed to count the harmonic uncertainty of the F3S measurement as:

$$U_c(k) = \left\{ \frac{1}{M_{simulate}} \sum_{i=1}^{M_{simulate}} \left[\left| G_{estimated,i}(jk) \right| - \frac{1}{M_{simulate}} \sum_{i=1}^{M_{simulate}} \left| G_{estimated,i}(jk) \right| \right]^2 \right\}^{1/2} \quad (22)$$

Here, U_c is the statistical harmonic uncertainty; $M_{simulate}$ is the simulation times, which equals 1000 in this paper, $G_{estimated,i}(jk)$ is the estimated Fourier coefficients of slide error motion.

Fig. 6 shows the comparison of the derived and the statistical harmonic uncertainty under the condition as subsection 4.1 described. Although there exists a maximal difference between the derived and the statistical harmonic uncertainty of 0.6 μm (6%) at the 28th harmonic, the derived uncertainties at almost each harmonic are well agreed with the statistical ones. This suggests that the derived uncertainties propagation law can quantify the influence of the spacing uncertainty in the F3S measurement.

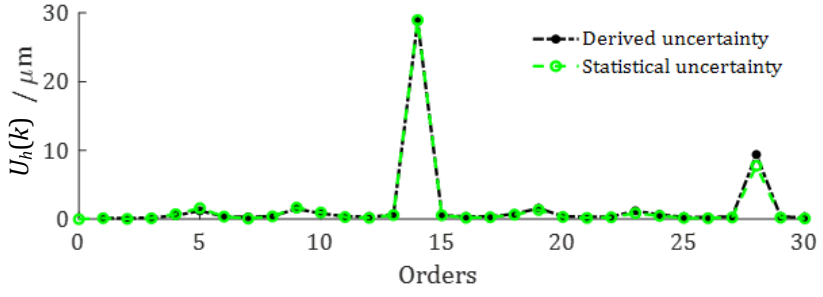

Fig. 6. The comparison of the derived and the statistical harmonic uncertainty.

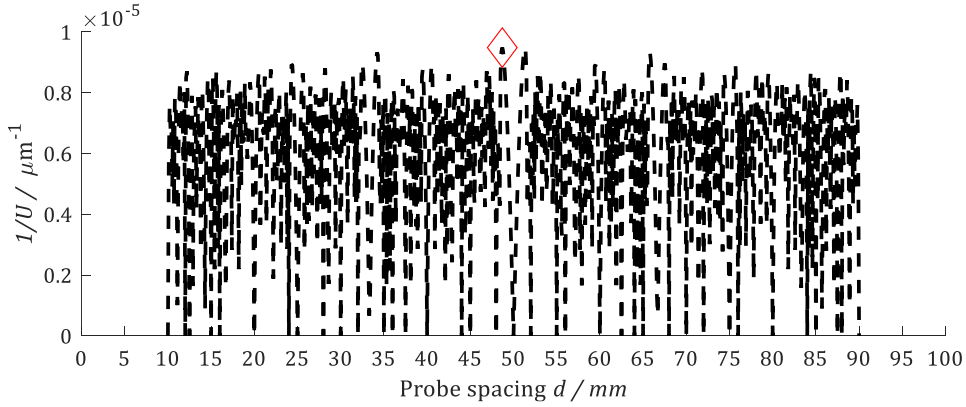

Fig. 7. The optimized spacing is defined via the derived harmonic uncertainty propagation law.

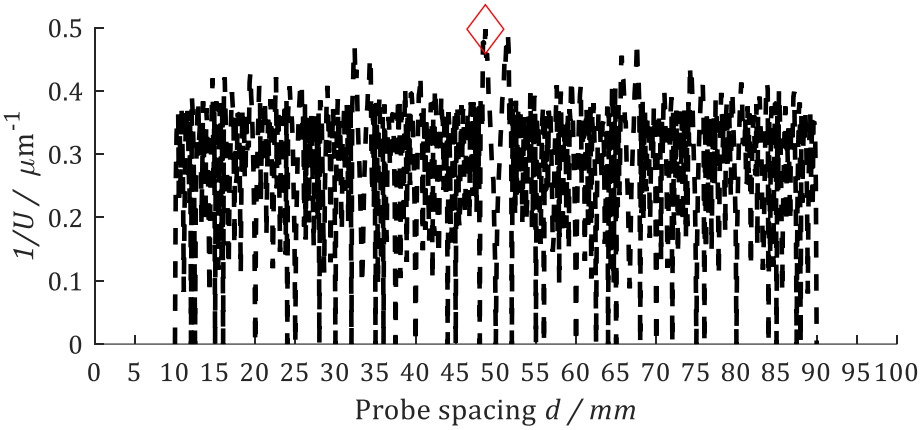

Fig. 8. The optimized spacing computed by Monte Carlo simulations.

4.4 Verification of probe spacing optimization based on the derived uncertainties propagation law

From Eq. (18), we can easily know that the F3S measurement uncertainty relates to the spacing d. Thus, a spacing d_{op} can be defined to achieve the smallest measurement uncertainty. To calculate the optimized spacing d_{op}, Eq. (19) was applied.

Due to the spacing error can cause significant measurement uncertainty, for convenient comparison, the reciprocal of measurement uncertainty is employed, as shown in Fig. 7. And the optimized d_{op} equals 48.7 mm, as marked by the red rhombus in Fig. 7.

Conventionally, to confirm the optimized spacing, Monte Carlo simulations were applied to compute the measurement uncertainty under all spacing d; then, find out the spacing d of the smallest measurement uncertainty in the spatial domain. The spatial measurement uncertainty can be described as:

$$U = \sqrt{\frac{1}{N_p M_{simulate}} \sum_{i_p=1}^{N_p} \sum_{i=1}^{M_{simulate}} \left(g_i(x_{i_p}) - g_{mean}(x_{i_p}) \right)^2} \quad (23)$$

where N_p is the total number of sampling points of the slide error motion.

With the same probe spacing uncertainty, the spatial measurement uncertainty under the spacing from 10 mm to 90 mm is calculated by conducting Monte Carlo simulations. For convenient demonstration, the reciprocal of measurement uncertainty is employed, as shown in Fig. 8. Thus, the optimized spacing, which also equals 48.7 mm, can be calculated at the maximal reciprocal of measurement uncertainty, where the smallest measurement uncertainty of 2.2 μm can be achieved, as marked by the red rhombus in Fig. 8. Thus, it suggests that, on the one hand, for enhancement of the F3S measurement precision, it is rational to optimize the spacing between the first and second probe based on the derived measurement uncertainty propagation law; on the other hand, it confirms the reliability of the uncertainty propagation law again.

5. Conclusions

(1) The adverse influence of the spacing deviation on the F3S measurement of slide error motion was theoretically analyzed.

(2) The probe spacing uncertainty propagation law in the F3S measurement, which can quantify the influence of the spacing uncertainty, was algebraically deduced by deriving the partial differential of the S function.

(3) To reduce the measurement uncertainty introduced by the spacing uncertainty, a method of optimizing the spacing d was proposed based on the uncertainty propagation law, which was verified by Monte Carlo simulations.

ACKNOWLEDGEMENT

This research is supported by the National Natural Science Foundation of China (Grant nos. 52175507 and 52375493), and the Natural Science Foundation of Guangdong Province (Grant nos. 2021A1515011687 and 2020A1515010807), and the Science and Technology Program of Guangzhou (Grant no. 2024A04J9928), which are highly appreciated by the authors.

REFERENCES

1. Yuan Y, Zhang D, Jing X, Zhu H, Zhu W, Cao J, Ehmann K. Fabrication of hierarchical freeform surfaces by 2D compliant vibration-assisted cutting. International Journal of Mechanical Sciences, 2019, 152: 454-464.
2. Suh S, Khurjekar P, Yang B, Characterization and identification of dynamic instability milling operation. Mechanical Systems and Signal Processing, 2002, 16(5): 853-872.
3. Fallah M, Moetakef-Imani B. Adaptive inverse control of chatter vibrations in internal turning operations. Mechanical Systems and Signal Processing, 2019, 129: 91-111.
4. Lu K, He Q, Xie J, Yang H, Chen Z, Ge D, Zhou C, Yin L. Nano-to-microscale ductile-to-brittle transitions for edge cracking suppression in single-diamond grinding of lithium metasilicate/disilicate glass-ceramics. Journal of the European Ceramic Society, 2023, 43(4), : 1698-1713.
5. Lu K, Chen Z, Luo Y, Huang P, He Q, Xie J, Yin L. Micro-grinding of lithium metasilicate/disilicate glass-ceramics. Ceramics International, 2022, 48(6): 8548-8562.
6. Liu C, Zhao C, Wen B. Dynamics analysis on the MDOF model of ball screw feed system considering the assembly error of guide rails. Mechanical Systems and Signal Processing, 2022, 178:

109290.

7. Patel T, Darpe A. Experimental investigations on vibration response of misaligned rotors. Mechanical Systems and Signal Processing, 2009, 23(7): 2236-2252.
8. Tan K, Huang S. Geometrical error compensation of machines with significant random errors. ISA Transactions, 2005 (44): 43–53.
9. Zhang H, Xiang S, Liu C, Sun J, Attifu K. Reverse identification of dynamic and static motion errors for five-axis machine based on specimen feature decomposition. ISA Transactions, 2022,
10. Whitehouse D. Some Theoretical Aspects of Error Separation Techniques in Surface Metrology. Journal of Physics E: Scientific Instruments, 1996, 9 (7):531-536.
11. Whitehouse D. Some theoretical aspects of error separation techniques in surface metrology. Journal of Physics E: Scientific Instruments, 1976, 9(7): 531-536.
12. Tanaka H, Tozawa K, Sato H, O-hori M, Sekiguchi H. Taniguchi N. Application of new straightness measurement method to large machine tool. CIRP Annals - Manufacturing Technology, 1981, 30(1): 455-459.
13. Tanaka H, Sato H. Extensive Analysis and Development of Straightness Measurement by Sequential-Two-Points Method. Journal of Engineering for Industry, 1986, 108(3): 176-182.
14. Li C., Li S, Yu J. High-resolution error separation technique for in-situ straightness measurement of machine tools and workpieces. Mechatronics, 1996, 6(3): 337-347.
15. Fung E, Yang S. An error separation technique for measuring straightness motion error of a linear slide. Measurement Science and Technology, 2000, 11: 1515-1521.
16. Huang P, Shi S, Xie J, Haitjema H, Niu Z, He Q, Lu K. On-machine workpiece straightness profile measurement using a hybrid Fourier 3-sensor method. Precision Engineering, 2023, 79: 190-199.
17. JCGM 101: 2008. Evaluation of measurement data – supplement 1 to the guide to the expression of uncertainty in measurement – propagation of distributions using a Monte Carlo Method.